Anal. Chem. **2004,** *76,* 2544−2552

Ultraflat Carbon Film Electrodes Prepared by Electron Beam Evaporation

Jason J. Blackstock,[†] Abbas A. Rostami,[‡,§] Aletha M. Nowak,[∥] Richard L. McCreery,[∥] Mark R. Freeman,[†] and Mark T. McDermott*[,‡]

Department of Physics and Department of Chemistry, University of Alberta, Edmonton, Canada, T6G2J1, and Department of Chemistry, The Ohio State University, Columbus, Ohio 43210

A facile method for the preparation of thin-film carbon electrodes by electron beam evaporation onto highly doped silicon is presented. The physical and electrochemical properties of these films both before and after postdeposition pyrolysis are investigated. Raman spectroscopy establishes the amorphous structure of the nonpyrolyzed carbon films and confirms the formation of graphitic carbon after pyrolysis at 1000 °C. Scanning force microscopy reveals the root-mean-square roughness of nonpyrolyzed films to be ∼1 Å, while pyrolyzed films exhibit an increased roughness of ∼4 Å. The electrochemical behavior of the electrodes resembles glassy carbon, with measured heterogeneous electron-transfer rate constants among the highest measured for thin carbon films. These carbon film electrodes will potentially find applications in such fields as molecular electronics and scanning probe microscopy of adsorbed species.

Due to a number of advantageous properties, carbon materials have been commonly employed in electroanalysis, electrocatalysis, and electrosynthesis.[1−3] In recent years, attention has been drawn to the fabrication of low-cost, disposable, carbon film electrodes for mass-scale use as electrochemical sensors.[4−7] Relatively thick films are commonly prepared by printing from commercial carbon ink.[5,8−10] These types of films often yield widely varying electrochemical reactivity due to binding polymers and other adhesion promoters present in the variety of carbon inks used.[7] Several methods have been reported for the fabrication of thin-film (≤400 nm) electrodes including chemical vapor deposition (CVD) of carbon containing gases,[11,12] sputtering,[13−16] electron-beam (e-beam) evaporation[17,18] and the pyrolysis of polymeric thin films.[19−23] In general, these thin film carbon electrodes are highly pure, contain some graphitic microstructure, are easily mass-produced, and yield electrochemical reactivity comparable to glassy carbon (GC).

Another characteristic of some carbon thin films that is proving useful for modern applications is surface flatness. Recently, the electrochemical reactivity of pyrolyzed photoresist film (PPF) electrodes, with an root-mean-square (rms) roughness of <1 nm, has been reported.[21,22] An exciting area of recent interest that requires extremely flat conductive surfaces is solid-state molecular electronics (moletronics). For example, a common approach to measure the electrical properties of metal−molecule−metal junctions is to sandwich a molecular layer between two mercury drops.[24,25] Ultraflat solid surfaces will be extremely important for future advancements of moletronic devices. Relevant to this work, McCreery et al. have recently shown that molecular layers covalently bound to carbon surfaces exhibit conduction switching and have interesting electrical properties.[26−29]

* To whom correspondence should be addressed. Voice: 780-492-3687. Fax: 780-492-8231. E-mail: mark.mcdermott@ualberta.ca.

[†] Department of Physics, University of Alberta.

[‡] Department of Chemistry, University of Alberta.

[§] On leave from the University of Mazandaran, Iran.

[∥] The Ohio State University.

(1) Kinoshita, K. *Carbon: Electrochemical and Physicochemical Properties*; Wiley: New York, 1988.

(2) McCreery, R. L. In *Electroanalytical Chemistry*; Bard, A. J., Ed.; Marcel Dekker: New York, 1991; Vol. 17, pp 221−374.

(3) McCreery, R. L. In *Interfacial Electrochemistry*; Wiekowski, A., Ed.; Dekker: New York, 1999; Chapter 35.

(4) Alvarez-Icaza, M.; Bilitewski, U. *Anal. Chem.* **1993**, *65*, 525A.

(5) Hart, J. P.; Wring, S. A. *Electroanalysis* **1994**, *6*, 617−624.

(6) Lindner, E.; Buck, R. P. *Anal. Chem.* **2000**, *72*, 336A−345A.

(7) Wang, J.; Tian, B. M.; Nascimento, V. B.; Angnes, L. *Electrochim. Acta* **1998**, *43*, 3459−3465.

(8) Wang, J.; Pamidi, P. V. A.; Park, D. S. *Anal. Chem.* **1996**, *68*, 2705−2708.

(9) Wang, J.; Pedrero, M.; Pamidi, P. V. A.; Cai, X. H. *Electroanalysis* **1995**, *7*, 1032−1034.

(10) Wang, J.; Pedrero, M.; Sakslund, H.; Hammerich, O.; Pingarron, J. *Analyst* **1996**, *121*, 345−350.

(11) Blaedel, W. J.; Mabbot, G. A. *Anal. Chem.* **1978**, *50*, 933−936.

(12) Eriksson, A.; Norekrans, A.-S.; Carlsson, J.-O. *J. Electroanal. Chem.* **1992**, *324*, 291−305.

(13) Sreenvas, G.; Ang, S. S.; Fritsch, I.; Brown, W. D.; Gerhardt, G., A.; Woodward, D. J. *Anal. Chem.* **1996**, *68*, 1858−1864.

(14) Fiaccabrino, G. C.; Tang, X.-M.; Skinner, N.; de Rooij, N. F.; Koudelka-Hep, M. *Sens. Actuators, B* **1996**, *35*−*36*, 247−254.

(15) Schlesinger, R.; Bruns, M.; Ache, H. J. *J. Electrochem. Soc.* **1997**, *144*, 6−15.

(16) You, T. Y.; Niwa, O.; Tomita, M.; Ichino, T.; Hirono, S. *J. Electrochem. Soc.* **2002**, *149*, E479−E484.

(17) DeAngelis, T. P.; Hurst, R. W.; Yacyncych, A. M.; Mark, H. B.; Heineman, W. R.; Mattson, J. S. *Anal. Chem.* **1977**, *49*, 1395−1398.

(18) Mattson, J. S.; Smith, C. A. *Anal. Chem.* **1975**, *47*, 1122−1125.

(19) McFadden, C. F.; Russell, L. L.; Melaragno, P. R.; Davis, J. A. *Anal. Chem.* **1992**, *64*, 1521−1527.

(20) Niwa, O.; Tabel, H. *Anal. Chem.* **1994**, *66*, 285−289.

(21) Ranganathan, S.; McCreery, R.; Majji, S. M.; Madou, M. *J. Electrochem. Soc.* **2000**, *147*, 277−282.

(22) Ranganathan, S.; McCreery, R. L. *Anal. Chem.* **2001**, *73*, 893−900.

(23) Singh, A.; Jayaram, J.; Madou, M.; Akbar, S. *J. Electrochem. Soc.* **2002**, *149*, E78−E83.

(24) Slowinki, K.; Fong, H. K. Y.; Majda, M. *J. Am. Chem. Soc.* **1999**, *121*, 7257−7261.

(25) Rampi, M. A.; Schueller, O. J. A.; Whitesides, G. M. *Appl. Phys. Lett.* **1999**, *72*, 1781−1783.

(26) Ranganathan, S.; Steidel, I.; Anariba, F.; McCreery, R. L. *Nano Lett.* **2001**, *1*, 491−494.

10.1021/ac035003j CCC: $27.50
Published on Web 03/27/2004

We report here a method for fabricating high-purity carbon films using e-beam evaporation directly onto flat, highly doped silicon wafers. Due to the nature of the deposition and the use of a high-purity carbon source, these e-beam deposited carbon films (ECFs) are expected to be highly pure. We examine the microstructure of ECFs with Raman spectroscopy before and after pyrolysis at 1000 °C. Importantly, nonpyrolyzed ECFs possess near-atomic-scale flatness. The electrochemical reactivity of ECFs is thoroughly characterized and compared to GC and other types of carbon thin films. These easily prepared, ultraflat films exhibit excellent electrochemical properties and should find uses in a wide variety of applications.

EXPERIMENTAL SECTION

Sample Preparation. Highly doped, ⟨100⟩ oriented, prime silicon wafers (N-type, arsenic doped; resistivity ≤40 Ω·mm; Silicon Valley Microelectronics) were diced into 1.5 × 1.5 cm sized substrates. The substrates were dipped in piranha solution (3:1 (v/v) concentrated H_2SO_4/30% H_2O_2), for 15 min to remove any organic surface contaminants. The native thermal oxide layer was then stripped from silcon wafers by immersion in 49% HF for exactly 1 min. Following a thorough rinse with deionized water and drying with nitrogen gas, the samples were loaded directly into the evaporation vacuum chamber. Safety note: HF and piranha solution are extremely corrosive and will severely burn unprotected skin.

The vacuum chamber evacuated to a pressure of $\sim 1 \times 10^{-6}$ Torr before evaporations and did not rise above 5×10^{-6} Torr during the deposition. A high-purity polycrystalline graphite source was located 17 in. from the sample holder. Evaporation rates were monitored with a quartz crystal microbalance. The beam current was adjusted to attain a deposition rate of 1 Å/s prior to opening the shutter between the sample and the source and occasionally fluctuated between the values of 0.5−2.5 Å/s throughout all evaporations. After evaporation, the samples were allowed to cool in a vacuum for upward of 1 h before the chamber was vented to nitrogen.

After removal from the chamber, "nonpyrolyzed" samples were evaluated with no further processing. For pyrolyzed films, samples were placed in a tube furnace and the atmosphere was flushed by forming gas (95% N_2 + 5% H_2). The gas flow was maintained at 100 sccm while the temperature was increased at the rate of 2 °C/min up to 1000 °C, held at 1000 °C for 1.5 h and then cooled to room temperature. The forming gas was kept flowing until the samples cooled to room temperature.[21]

Physical/Chemical Characterization. The adhesion of the carbon films to the Si substrate was tested by the "tape test" as describe in ASTM D3359-02 Standard Test Methods for Measuring Adhesion by Tape Test. This test consists of pressing an adhesive tape onto the surface of a film and then pulling the tape away. Poorly adhered films will peel away from the substrate with the tape, whereas well-adhered films will be undisrupted. The resistivity of the carbon films was determined by measuring the sheet resistance by four probe measurements and calculating the resistivity.

Raman spectra were collected with a line-focused $f/2$ Raman spectrometer (Chromex) and a back-thinned CCD (Andor), described previously.[30] A 514.5-nm argon ion laser (Coherent) with a power of 50 mW at the sample was used. The laser was incident on the sample at 45° and collection at 0° with respect to the surface normal. The focal line was approximately 5 mm × 50 μm and was generated by a Powell lens (Lasiris, P-5°, Lasiris, Inc., Quebec, Canada). Integration time was 30 s for the 200-nm film and 120 s for the 7-nm film. Spectra are displayed as an average of 10 integrations. Spikes in CCD integrations were removed by comparing successive spectra and rejecting intensities that exceeded those in previous spectra by more than 200 CCD digitizer units.

Scanning force microscopy (SFM) was carried out using both Multimode and Dimension 3000 microscopes from Digital Instruments (Santa Barbra, CA). In all cases, the SFM images were collected in contact mode with scan rates of 1−5 Hz using commercial Si_3N_4 cantilevers (k = 0.6 nN/nm; ThermoMicroscope). Nonpyrolyzed samples were examined immediately after removing the samples from the evaporation chamber, and pyrolyzed samples were examined after removal from the furnace. At least five different measurements from randomly selected points across a sample were averaged to provide the given result. Also, at least one other sample of each type was briefly examined to ensure the observed values were reproducible. For thickness measurement, images were collected at the boundary between the film and the region blocked by the clip used to hold the substrate in place.

Electrochemical Characterization. Reagents and solvents used included the following: sulfuric acid (Mallinckrodt Inc.); sodium perchlorate (Fisher); potassium chloride (Fisher); hydrofluoric acid (Backer Chemical Co.); hydrogen peroxide (Merck); perchloric acid (Caledon); *n*-tetrabutylammonium terafluoroborate(Aldrich); 2-propanol (IPA, Mallinckrodt Inc.); acetonitrile (Mallinckrodt Inc.); anthraquinone-2,6-disulfonate (2,6-AQDS) sodium salt (Aldrich); activated carbon (Darco S-51, Norit Inc.). All chemicals were reagent grade and were used as received. Solutions were prepared fresh daily and degassed with ultrapure (99.99%) nitrogen gas for 10 min before use. Aqueous solutions were prepared in water purified first by reverse osmosis and then deionized through a Millipore system (Nanopure water, 18 MΩ cm^{-1}).The redox systems examined were as follows: 1 mM $Fe(CN)_6^{3-}$ in 1 M KCl from $K_3Fe(CN)_6$ (BDH Chemicals); 1 mM $[Ru(NH_3)_6]^{3+}$ in 1 M KCl from $Ru(NH_3)_6Cl_3$ (Aldrich); 5 mM Eu^{3+} (aquated) in 0.2 M $NaClO_4$ from $Eu(NO_3)_3 \cdot 5H_2O$ (Aldrich); 1 mM dopamine (DA, Sigma) in 0.1 M H_2SO_4; 1 mM ferrocene (Fc, Fluka) in acetonitrile containing 0.1 M *n*-tetrabutylammonium terafluoroborate.

Prior to electrochemical experiments, all samples were sonicated in a mixture of 50:50 (v/v) 2- propanol/acetonitrile with an equal volume of activated carbon for 10 min. The electrodes were then sonicated in deionized water (Nanopure, 18 MΩ) for 10 min. Electrochemical measurements were performed using a computer-controlled bipotentiostat (model AFCBP1; Pine Instruments). A three-electrode cell was used with Ag/AgCl/KCl (sat) as reference electrode and a Pt wire as a counter electrode. The surface area

(27) Solak, A. O.; Ranganathan, S.; Itoh, T.; McCreery, R. L. *Electrochem. Solid State Lett.* **2002**, *5*, E43−E46.
(28) Anariba, F.; McCreery, R. L. *J. Phys. Chem. B* **2002**, *106*, 10355−10362.
(29) Solak, A. O.; Eichorst, L. R.; Clark, W. J.; McCreery, R. L. *Anal. Chem.* **2003**, *75*, 296−305.
(30) Ramsey, J.; Ranganathan, S.; McCreery, R. L.; Zhao, J. *Appl. Spectrosc.* **2001**, *55*, 767−773.

of working electrode was defined by an elastometric O-ring and electrochemically determined to be 0.35 ± 0.01 cm^2.

Heterogeneous electron-transfer (ET) rate constants were determined from the anodic/cathodic peak separation using the method of Nicholson[31] by assuming $\alpha = 0.5$ and using the following diffusion coefficients: $Fe(CN)_6^{3-/4-}$, $D_O = 7.63 \times 10^{-6}$ cm^2 s^{-1}, $D_R = 6.32 \times 10^{-6}$ cm^2 s^{-1}; $[Ru(NH_3)_6]^{3+/2+}$, $D_O = 6.5 \times 10^{-6}$ cm^2 s^{-1}; $Eu^{3+/2+}$ (aquated), $D_O = 7.9 \times 10^{-6}$ cm^2 s^{-1}; ferrocene, $D_O = 2.4 \times 10^{-5}$ cm^2 s^{-1}; dopamine, $D_O = 6.0 \times 10^{-6}$ cm^2 s^{-1}. In all cases except for $Fe(CN)_6^{3-/4-}$, it was assumed that $D_R = D_O$ for rate constant calculations. Double layer capacitance of ECFs in 1 M KCl solutions were determined using cyclic voltammetry. For 2,6-AQDS adsorption measurements, cyclic voltammograms of 10 μM 2,6-AQDS in 1 M $HClO_4$ at a scan rate of 100 mV s^{-1} were obtained after an adsorption time of 10 min. Surface coverage of 2,6-AQDS was quantified by measuring the area under the voltammetric reduction wave as described by Brown and Anson.[32]

RESULTS

Physical Characterization. *Film Thickness.* The quartz crystal used to monitor the rate of deposition was also used to determine the final thicknesses of the deposited carbon films. For several nonpyrolyzed samples, SFM was used to confirm that the quartz crystal values were accurate. The thicknesses reported by the crystal generally agreed with SFM measured thickness to within 5%. The thicknesses quoted in this paper are those measured by the quartz crystal monitor. For the majority of the characterizations, the two ECF thicknesses examined were 7 and 200 nm. In SFM roughness characterizations, several other film thicknesses were also examined. Recent reports have demonstrated that pyrolysis of carbon films at temperatures of ≥1000 °C in oxygen-free, hydrogen-containing atmosphere improves electrochemical performance.[21] SFM was also used to measure the thickness of several pyrolyzed samples. These thicknesses were compared against the AFM thickness values of nonpyrolyzed samples prepared in the same evaporation run. We found that pyrolysis results in no notable change in the thickness. This observation is notable because pyrolysis of photoresist films under similar conditions results in significant reduction of mass.[21]

Film Adhesion. Evaporated carbon films are known to have poor adhesion to many clean surfaces.[18,33] For example, we observed very poor adhesion to the internal glass and stainless steel in our evaporation chamber. Conventionally, secondary layers comprising materials such as titanium are deposited to promote adhesion of the carbon films to the underlying substrate.[15] The ECFs prepared in this work passed the tape test, indicating strong adhesion between the carbon and the oxide-free silicon. We attribute the source of this adhesion to the formation of a thin silicon carbide (SiC) layer at the interface between the film and the silicon substrate. The formation of this layer upon electron beam evaporation of carbon directly onto an oxide-free silicon surface has been previously observed and studied by X-ray photoelectron spectroscopy (XPS).[34] Note that, immediately prior to loading, our substrates are immersed in hydrofluoric acid. which strips away the native oxide layer and generates a hydrogen-terminated Si surface. Carbon is therefore evaporated onto an oxide-free surface allowing direct interaction with hydrogen-terminated silicon. The flux of carbon atoms likely desorbs the surface hydrogen to form a SC layer that we anticipate to be on the order of 1 nm thick.

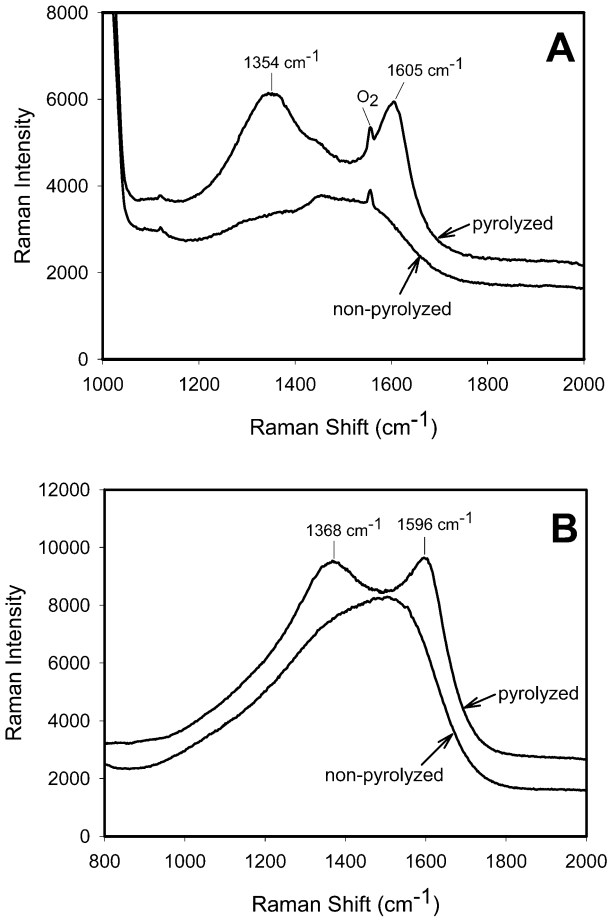

Figure 1. Raman spectra for (A) 7- and (B) 200-nm ECF.

Film Resistivity. One of the challenges in previous attempts to use electron beam-deposited carbon films as electrodes was high resistivity.[17,18] Mattson and co-workers measured sheet resistances for 300-nm-thick ECFs in the range of 2000−5000 Ω/□,[18] considerably higher than the resistance values of typical electrodes. To eliminate any problems arising from a high ohmic resistance of the films, highly doped-silicon (resistivity ≤40 Ω·μm) was employed as the substrate underlying the carbon films. The SiC layer responsible for good observed adhesion should also provide good electrical contact between the ECFs and the underlying conductive silicon. This is based on the observed electrical properties of silicon carbides.[35] The sheet resistance measured for both freshly cleaned silicon and all ECFs was 0.04 Ω/□. For a wafer thickness of 500 μm, we calculate a resistivity of 20×10^{-4} Ω·cm, in good agreement with the supplier specifications. This observation indicates that the flow of electrical current along the length of the electrode is dominated by paths through the silicon. Uncompensated resistance in electrochemical measurements was determined via electrochemical means as described below.

Raman Spectroscopy. Raman spectroscopy was employed to probe the microstructure of the ECFs. Representative results in

(31) Nicholson, R. S. *Anal. Chem.* **1965**, *37*, 1351.
(32) Brown, A. P.; Anson, F. C. *Anal. Chem.* **1977**, *49*, 1589−1595.
(33) *Thin Film Evaporation Source Reference*; R. D. Mathis Co.: Long Beach, CA, 1987.
(34) Luthin, J.; Linsmeier, C. *Phys. Scr.* **2001**, *T91*, 134−137.

the 1000−2000-cm^{-1} region are shown in Figure 1. Figure 1A contains Raman spectra for 7-nm ECFs before and after pyrolysis at 1000 °C for 1 h. In both spectra, the intense band at ∼1000 cm^{-1} is due to the Si substrate. A number of bands characteristic of Si are observed below 1000 cm^{-1} due to the large penetration depth of the Ar^+ laser (∼25 nm) relative to the carbon film thickness. The spectrum of the 7-nm nonpyrolyzed EDF shows a broad feature centered at ∼1500 cm^{-1} that is diagnostic of amorphous carbon. This Raman spectrum is qualitatively similar to those in previous reports of carbon films deposited at room temperature by e-beam evaporation[36] and sputtering.[15] Following pyrolysis, distinct bands appear that are characteristic of a graphitic structure. The band at 1605 cm^{-1} is assigned as the G band commonly observed in graphitic material. The position of this band in Figure 1A is blue shifted from the position of this band in graphite (∼1582 cm^{-1}) as has been observed for carbon films with extremely small microcrystallite size.[37] Also observed is the D band at 1354 cm^{-1}, which is diagnostic of disorder in carbon materials.[38] Thin carbon films formed by pyrolysis of photoresist layers also exhibit G and D bands for pyrolysis temperatures over 600 °C. The poor resolution of the G and D bands in Figure 1A and the D/G intensity ratio of ∼1 also imply that, although pyrolysis results in some graphite microcrystallite formation, the carbon layer comprising the pyrolyzed 7-nm ECFs is an extremely disordered material.

Raman spectra for 200-nm ECFs are shown in Figure 1B. In this case, the thickness of film is sufficient to shield Raman scattering from the Si substrate. Qualitatively, the results for the 200-nm films are identical to those for the 7-nm films. That is, the nonpyrolyzed ECFs exhibit an amorphous structure. Pyrolysis of the films at 1000 °C induces limited graphitization and results in a film with a disordered graphitic structure.

Surface Topography. Nonpyrolyzed ECFs with a range of thicknesses were examined to determine how increasing deposition thickness influences surface morphology. Shown in Figure 2A are the SFM determined root-mean-square (rms) roughness values determined from image sizes of 100 × 100 nm and 1 × 1 μm. The rms values of all the films 7 nm and thicker are between 0.7 and 1.1 Å. These values are very close to the 0.6-Å rms roughness measured over both length scales for the underlying silicon ⟨100⟩ surface. The slightly higher roughness of the 2-nm films, particularly at the larger scan size, is likely due to initial island formation of the carbon film on the surface prior to complete coverage.

Figure 2B compares the roughness of pyrolyzed to nonpyrolyzed ECFs of 7- and 200-nm thickness. Clearly, from the results, pyrolysis of the films results in a considerable increase in roughness at both length scales. This increase in roughness may be correlated with the Raman results demonstrating increased graphitization with pyrolysis; the formation of independently oriented graphitic domains in the films can be expected to disrupt the originally flat surface. Despite the increased roughness, however, the actual values of between 3 and 6 Å still represent an exceedingly flat surface. The rms values for the pyrolyzed ECFs are similar to that measured at PPF surfaces, which are pyrolyzed under similar conditions.[22] Several images were also collected on samples at length scales up to and exceeding dimensions of 10 × 10 μm. The roughness measured in these images was similar to that of the 1 × 1 μm^2 scans, demonstrating that electrode flatness extends over a long-range and is not a local effect.

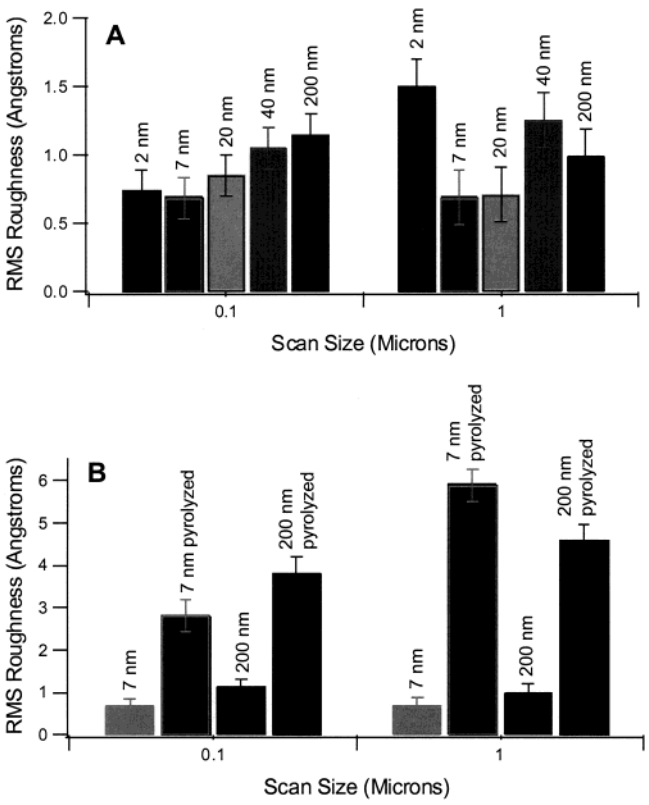

Figure 2. Bar graphs of SFM measured rms roughness as a function of image size. (A) Results from a variety of films thickness for nonpyrolyzed films. (B) Results for 7- and 200-nm films before and after pyrolysis.

To better illustrate the topography of the ECF surfaces, Figure 3 presents an assembly of contact-mode SFM images for 7- and 200-nm films at image sizes of 100 × 100 nm^2 and 1 × 1 μm^2. Note that the black-to-white vertical scale on these images is only 5 nm. The left column displays images of nonpyrolyzed samples (A, C, E, G), whereas the right column displays the respective images for the pyrolyzed samples (B, D, F, H).

The nonpyrolyzed films exhibit an extremely flat and featureless topography over both length scales presented. Pyrolysis of the films results in a more textured surface as reflected in the rms values in Figure 2B. Comparing the 1 × 1 μm images of nonpyrolyzed ECFs to the pyrolyzed (7 nm, A and B; 200 nm, E and F), features with lateral dimensions in the hundreds of nanometers and heights of 1−2 nm are observed to develop due to pyrolysis. In the higher resolution 100 × 100 nm^2 images (7 nm, C and D; 200 nm, G and H), vertical variations of <1 nm occur smoothly over a smallest lateral length scale of tens of nanometers.

Electrochemical Characterization. The electrochemical reactivity of the ECFs was assessed by measuring ET rates, capacitance, and adsorption. Several redox systems, chosen because of their varying sensitivity to carbon surface structure,

(35) Pensl, G.; Choyke, W. J. *Physica B* **1993**, *185*, 264−283.
(36) Schelz, S.; Richmond, T.; Kania, P.; Oelhafen, P.; Guntherodt, H. J. *Surf. Sci.* **1996**, *359*, 227−236.
(37) Besold, J.; Thielsch, R.; Matz, N.; Frenzel, C.; Born, R.; Mobius, A. *Thin Solid Films* **1997**, *293*, 96−102.
(38) Wang, Y.; Alsmeyer, D. C.; McCreery, R. L. *Chem. Mater.* **1990**, *2*, 557−563.

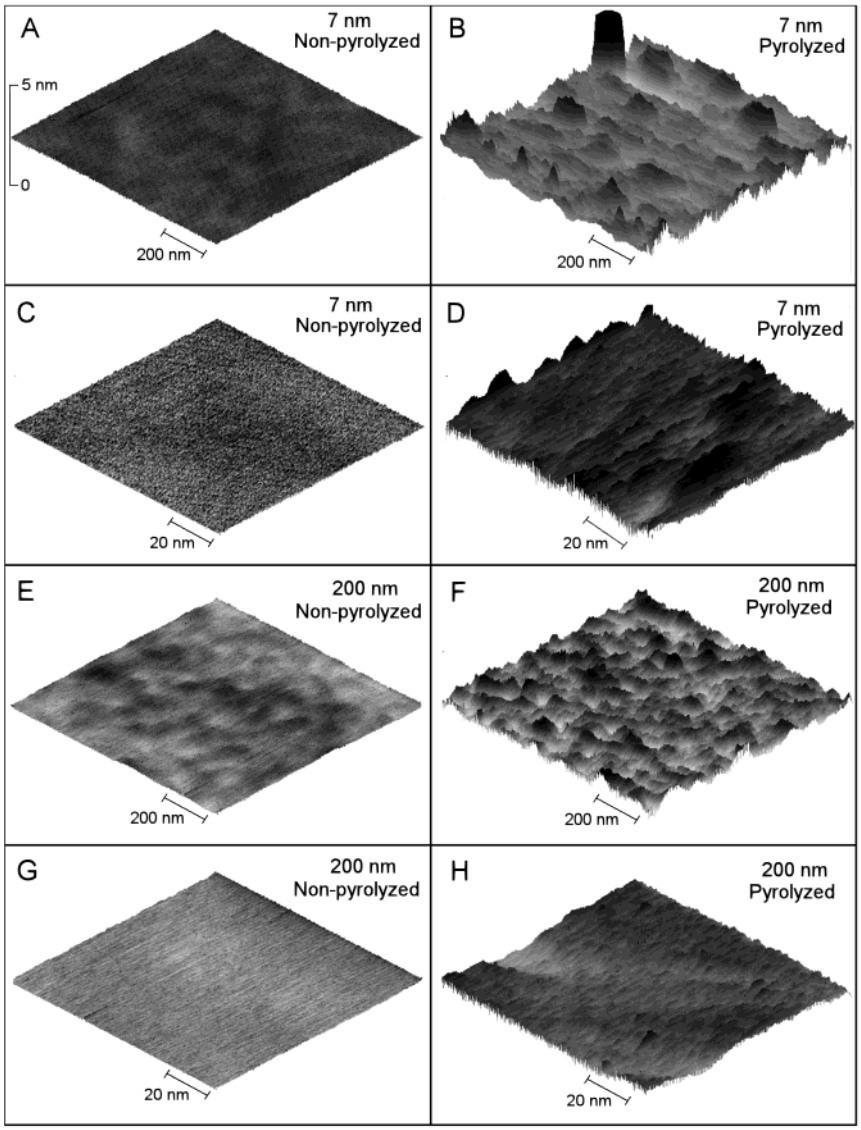

Figure 3. Surface plot presentation of contact-mode SFM imaged of ECFs. The *z*-scale bar in (A) applies to all images. (A) $1 \times 1\ \mu m^2$ image of a nonpyrolyzed 7-nm film. (B) $1 \times 1\ \mu m^2$ image of a pyrolyzed 7-nm film. (C) $100 \times 100\ nm^2$ image of nonpyrolyzed 7-nm film. (D) $100 \times 100\ nm^2$ image of a pyrolyzed 7-nm film. (E) $1 \times 1\ \mu m^2$ image of a nonpyrolyzed 200-nm film. (F) $1 \times 1\ \mu m^2$ image of a pyrolyzed 200-nm film. (G) $100 \times 100\ nm^2$ image of a nonpyrolyzed 200-nm film. (H) $100 \times 100\ nm^2$ image of a pyrolyzed 200-nm film.

were used to probe ET. Figure 4A contains uncorrected cyclic voltammograms for 1 mM $Fe(CN)_6^{3-/4-}$ (1 M KCl, $\nu = 500$ mV/s) on 200-nm ECFs, polished GC, and doped Si substrate. The highly doped Si substrate exhibits negligible ET reactivity due to the presence of an insulating native oxide layer. As discussed below, some of the films investigated here are very thin (e.g., 7 nm) and may contain small pinholes exposing the underlying substrate. Although we have no direct evidence for pinholes, their existence will not influence the observed electrochemical response due to the negligible reactivity of the Si substrate observed in Figure 4A. The current−potential curves in Figure 4 also show that the pyrolyzed 200-nm ECF ($\Delta E_p = 83$ mV) and polished GC ($\Delta E_p = 90$ mV) exhibit very similar ET characteristics while the nonpyrolyzed 200-nm ECF provides a lower ET rate ($\Delta E_p = 120$ mV).

The data from voltammograms of 1 mM $Fe(CN)_6^{3-/4-}$ (1 M KCl) at a range of scan rates for 7- and 200-nm pyrolyzed ECFs are listed in Table 1. In each case, peak current is linear with $\nu^{1/2}$ and the ratio of cathodic to anodic peak current is ~1 for all scan rates. In addition, the observed ΔE_p increases with scan rate. Similar results are obtained at nonpyrolyzed films. These observations imply that $Fe(CN)_6^{3-/4-}$ is behaving as a semi-infinite linear diffusion-controlled system with quasi-reversible ET kinetics at ECFs, which is consistent with observations at most carbon electrode materials such as GC. Observed heterogeneous electron-transfer rate constants, k°_{obs}, were determined from ΔE_p values via the method of Nicholson and are also listed in Table 1. Although the variation in k° for each sample is reasonable, both films show a decrease in the observed k° as the scan rate is increased. This type of behavior reflects a significant uncompensated cell resistance.

A previous report[22] detailing the properties of PPF electrodes noted that the effect of film resistance on the observed ΔE_p can be corrected by applying the following equation,

$$\Delta E_{p,corr} = \Delta E_{p,obs} - 2|i|R_u$$

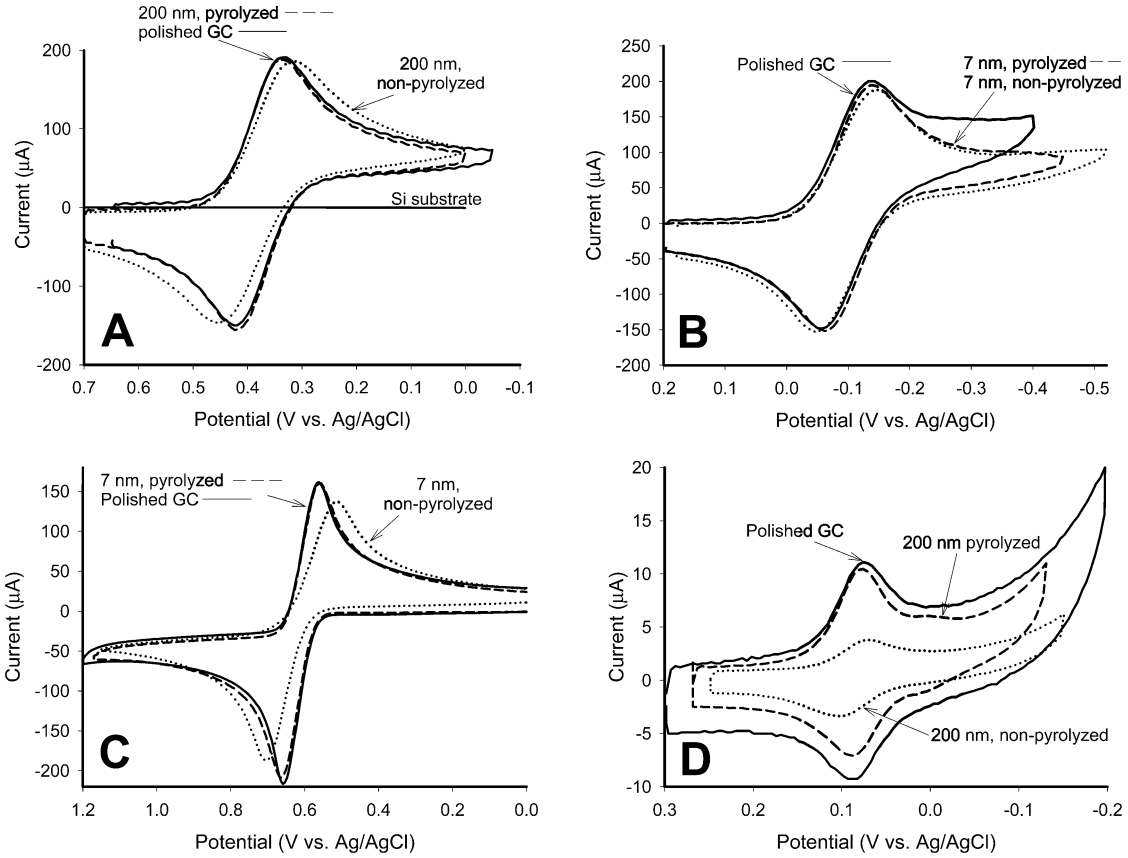

Figure 4. Cyclic voltammetric results for several redox systems on ECFs and GC. (A) 1 mM $Fe(CN)_6^{3-}$ (1 M KCl), $\nu = 500$ mV/s. (B) 1 mM $Ru(NH_3)_6^{3+}$ (1 M KCl), $\nu = 500$ mV/s. (C) 1 mM dopamine (0.1 M H_2SO_4), $\nu = 200$ mV/s. (D) 10 μM 2.6-AQDS (1 M $HClO_4$), $\nu = 100$ mV/s.

Table 1. Detailed Data from Cyclic Voltammetry of $Fe(CN)_6^{3-/4-}$

electrode	scan rate (mV/s)	i_c (μA)	i_c/i_a	$\Delta E_{p,meas}$ (mV)	$k°_{meas}$ (cm/s)	$\Delta E_{p,corr}$[a] (mV)	$k°_{corr}$ (cm/s)
7-nm pyrolyzed ECF	100	83	1.05	81	0.011	70	0.022
	200	113	1.04	88	0.011	73	0.024
	500	173	1.05	100	0.011	77	0.029
	1000	233	1.06	121	0.0097	90	0.022
	2000	316	1.08	138	0.0094	96	0.026
	4000	422	1.14	169	0.010	112	0.022
200-nm pyrolyzed ECF	100	86	1.01	67	0.031	60	rev[b]
	200	120	1.00	75	0.023	65	0.062
	500	188	1.03	83	0.022	67	0.069
	1000	260	1.01	96	0.019	74	0.051
	2000	367	1.04	111	0.017	80	0.055
	4000	518	1.07	129	0.016	85	0.050

[a] Corrected for iR error. [b] Indicates that ΔE_p is very close to the reversible limit and no attempt was made to quantify $k°$.

where $\Delta E_{p,corr}$ is the corrected ΔE_p (in V), i is the voltammetric peak current (in A), and R_u is the uncompensated cell resistance (in Ω). R_u can be determined from the slope of a plot of $\Delta E_{p,obs}$ versus i from voltammograms at a common scan rate for solutions of varying concentrations. Data from CV experiments collected on 7- and 200-nm pyrolyzed ECFs in solutions of $Fe(CN)_6^{3-/4-}$ with concentrations between 1 and 10 mM are plotted in Figure 5. Analysis of a number of these plots on different films yields R_u values of 63 ± 6 and 44 ± 3 Ω for the 7- and 200-nm films, respectively. For a given film thickness, we obtain similar R_u values for both nonpyrolyzed and pyrolyzed films. We believe this is due the dominance of the highly doped, conductive Si substrate on the overall sample resistance. Also listed in Table 1 are ΔE_p values corrected for iR_u error ($\Delta E_{p,corr}$) and their corresponding $k°$ values. All $k°$ values discussed hereafter have been corrected for sample resistance.

Figure 4 also presents examples of uncorrected voltammetry for other redox systems on ECFs. Figure 4B contains current−potential curves for $Ru(NH_3)_6^{2+/3+}$ (1 M KCl, $\nu = 500$ mV/s) on 7-nm ECFs and polished GC. Well-behaved voltammetry characteristic of a redox system with quasi-reversible ET kinetics is observed for $Ru(NH_3)_6^{2+/3+}$ on all ECFs. Importantly, the volatmmetry of $Ru(NH_3)_6^{2+/3+}$ on ECFs is comparable to that on GC. Figure 4C contains current−potential curves for dopamine (0.1 M H_2SO_4, $\nu = 200$ mV/s) on 7-nm ECFs and polished GC. Once again, qualitatively similar voltammetry is observed at ECFs

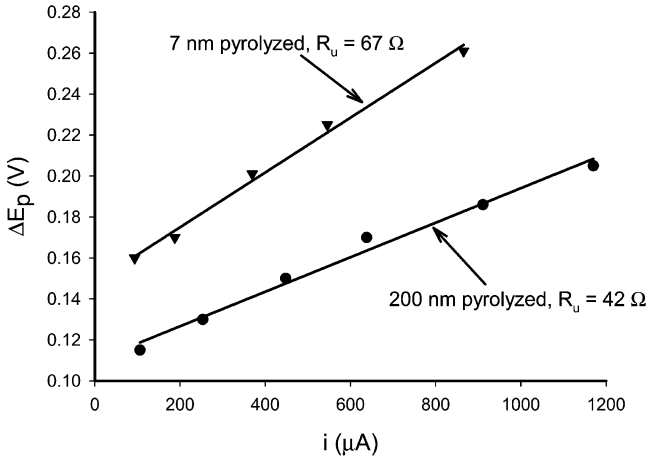

Figure 5. Plots of ΔE_p vs peak current from cyclic voltammetry (ν = 100 mV/s) of $Fe(CN)_6^{3-}$ (1 M KCl) at ECFs. The concentration of $Fe(CN)_6^{3-}$ was varied from 1 to 10 mM to affect the different peak currents. The slope of each least-squares, linear fit yields $2R_u$.

compared to polished GC. In this case, GC (ΔE_p = 107 mV) and the pyrolyzed 7-nm film (ΔE_p = 113 mV) yield faster ET rates for DA than the nonpyrolyzed 7-nm film (ΔE_p = 199 mV). Finally, the voltammetry of surface bound 2,6-AQDS on 200-nm ECFs and polished GC is shown in Figure 4D. In these experiments, the electrodes were immersed in 10 μM 2,6-AQDS (1 M $HClO_4$) and the voltammograms were collected after the adsorbed layer had reached equilibrium with the contacting solution (~10 min). In all cases, near-ideal voltammetric waves characteristic of an adsorbed redox species are observed. Overall, all ECFs examined yielded voltammetry for both solution-bound and adsorbed species that was qualitatively similar to that observed at GC.

Table 2 summarizes our electrochemical characterizations of ECFs more quantitatively and lists some comparative values for GC. In some cases, several $k°$ values at GC are listed to present laboratory-to-laboratory variations. A similar extensive electrochemical characterization on PPF has recently appeared enabling a direct comparison. Thus, values for most of the parameters examined are also listed for PPF electrodes. It should be noted that all electrodes used in this work (ECF and GC) were treated with activated carbon/isopropyl alcohol as were all surfaces reported in ref 22. This treatment has been shown to significantly lower the amount of organic impurities on carbon electrodes.[39]

In addition to $Fe(CN)_6^{3-/4-}$, $Ru(NH_3)_6^{2+/3+}$, and DA, we also explored the ET kinetics of the aquated $Eu^{2+/3+}$ species in aqueous electrolyte and Fc in acetonitrile. As noted above, the systems studied were chosen because of their specific dependence on the surface state of carbon electrodes. The ET rate for $Fe(CN)_6^{3-/4-}$ at carbon electrodes is very sensitive to surface preparation procedures[40] while the outer-sphere $Ru(NH_3)_6^{3+/2+}$ and Fc systems are insensitive to surface state.[41] The $Eu^{3+/2+}$ system has been shown to be very sensitive to the presence of surface carbonyl groups at carbon electrodes.[42,43] Finally, facile DA oxidation involves adsorption of reactant to oxide-free sites at carbon electrodes.[44]

The ET reactivity of ECF can be evaluated and compared to GC and PPF by considering the $k°$ values for the 1-electron redox systems and the ΔE_p values for DA. In terms of ET rates, we generally obtain poor reproducibility at nonpyrolyzed ECFs as evidenced by their large relative standard deviations (RSDs). Pyrolyzed films exhibit RSD values as good or better that polished GC in most cases. The magnitude of $k°$ at the nonpyrolyzed films is comparable to that observed at GC and PPF for the systems studies. Pyrolysis of the films generally increases $k°$. For example, for both film thickness, $k°$ for $Fe(CN)_6^{3-/4-}$ is a factor of 5 higher at pyrolyzed relative to nonpyrolyzed films. We attribute this enhancement in ET reactivity to the graphitization induced by pyrolysis.

With respect to the individual redox systems, $k°$ values for $Fe(CN)_6^{3-/4-}$, $Ru(NH_3)_6^{3+/2+}$, and Fc at ECFs are very similar and in some cases slightly higher than that observed at GC. The comparable $k°$ values for $Eu^{2+/3+}$ at ECFs and polished GC listed in Table 2 imply a similar amount of surface oxides. Polished GC generally exhibits an O/C ratio as determined by XPS of ~8%.[22,45] The O/C ratio at PPF starts at ~2% and increases to ~6% with air exposure.[22] Although we have not performed XPS analysis on ECF, the $Eu^{2+/3+}$ results after 1−2 days in the laboratory environment indirectly imply that the O/C ratio is between 5 and 10%. Table 2 also shows that pyrolysis of ECFs lowers the ΔE_p for DA. We believe that the modest amount of graphitization induced during pyrolysis increases the density of surface sites necessary for DA to adsorb and, thus, oxidize at a higher rate. This is supported by the observation that GC, which is composed of almost exclusively sp^2 hybridized carbon in the form of graphite microcrystallites, yields significantly lower ΔE_p values for DA.

The results from 2,6-AQDS adsorption experiments in Table 2 provide additional evidence for an increase in adsorption sites with pyrolysis. It has been shown that 2,6-AQDS adsorbs irreversibly at carbon electrodes and exhibits near-ideal behavior for a surface-bound redox species.[46,47] The theoretical saturation coverage for 2,6-AQDS adsorbing with rings parallel to a flat surface is 132 pmol/cm^2.[48] As indicated in Table 2, significantly less than a monolayer of 2,6-AQDS is measured at nonpyrolyzed films. Either the amorphous structure of the nonpyrolyzed film does not provide a high density of adsorption sites or 2,6-AQDS adsorbs in a nonelectroactive orientation. Interestingly, a similar coverage is measured at PPF electrodes. The pyrolyzed ECFs yield coverages that approach a theoretical monolayer. The increase in roughness shown in Figure 3 for pyrolyzed films likely contributes to the higher coverage. In addition, we believe that the graphitization of the films induced by pyrolysis increases the density of adsorption sites for 2,6-AQDS, an assertion also consistent with the DA results.

(39) Ranganathan, S.; Kuo, T. C.; McCreery, R. L. *Anal. Chem.* **1999**, *71*, 3574−3580.
(40) McCreery, R. L.; Cline, K. K.; McDermott, C. A.; McDermott, M. T. *Colloid Surf. A* **1994**, *93*, 211−219.
(41) Chen, P. H.; McCreery, R. L. *Anal. Chem.* **1996**, *68*, 3958−3965.
(42) McDermott, C. A.; Kneten, K. R.; McCreery, R. L. *J. Electrochem. Soc.* **1993**, *140*, 2593−2599.
(43) Chen, P. H.; Fryling, M. A.; McCreery, R. L. *Anal. Chem.* **1995**, *67*, 3115−3122.
(44) DuVall, S. H.; McCreery, R. L. *J. Am. Chem. Soc.* **2000**, *122*, 6759−6764.
(45) Kiema, G. K.; Aktay, M.; McDermott, M. T. *J. Electroanal. Chem.* **2003**, *540*, 7−15.
(46) McDermott, M. T.; Kneten, K.; McCreery, R. L. *J. Phys. Chem.* **1992**, *96*, 3124−3130.
(47) McDermott, M. T.; McCreery, R. L. *Langmuir* **1994**, *10*, 4307−4314.
(48) Soriaga, M. P.; Hubbard, A. T. *J. Am. Chem. Soc.* **1982**, *104*, 3937.

Table 2. Electrochemical Results for ECFs, GC and PPF

surface	k° (cm/s)[a] $Fe(CN)_6^{3-/4-}$ (1 M KCl)	k° (cm/s)[a] $Ru(NH_3)_6^{3+/2+}$ (1 M KCl)	k° (cm/s)[a] $Eu_{aq}^{3+/2+}$ (0.2 M $NaClO_4$)	k° (cm/s)[a] Fc/Fc^+ In CH_3CN (0.1 M $TBABF_3$)	ΔE_p (mV) $\nu = 200$ mV/s DA (0.1 M H_2SO_4)	C° (μF/cm^2) (1 M KCl)	$\Gamma_{2,6-AQDS}$ (pmol/cm^2) (1 M $HClO_4$)
7 nm	2.7×10^{-3} (15%)[b]	1.9×10^{-2} (20%)	6.3×10^{-4} (50%)	1.3×10^{-3} (38%)	227 ± 25 ($N = 2$)	17 ± 3 ($N = 3$)	28
7 nm (py)	1.4×10^{-2} (25%)	4.6×10^{-2} (17%)	6.0×10^{-4} (47%)	2.4×10^{-3} (12%)	119 ± 6 ($N = 2$)	14 ± 2 ($N = 4$)	105
200 nm	5.7×10^{-3} (17%)	2.7×10^{-2} (22%)	5.3×10^{-4} (50%)	2.1×10^{-3} (30%)	243 ± 13 ($N = 3$)	21 ± 8 ($N = 3$)	30
200 nm (py)	2.9×10^{-2} (14%)	4.3×10^{-2} (14%)	6.0×10^{-4} (50%)	2.2×10^{-3} (14%)	130 ± 4 ($N = 3$)	25 ± 1 ($N = 4$)	123
polished GC	8×10^{-3} (25%)[c] 3.4×10^{-2}[e]	1.9×10^{-2} (11%)[c] 1.7×10^{-2}[d] 3.7×10^{-2}[e]	3.2×10^{-4} (38%)[c]	1.8×10^{-3}[d]	107[d] 74[e] 67[f]	34 ± 2[d] 41[c]	172[c]
PPF	1.2×10^{-2}[e]	2.0×10^{-2}[e]			287[e]	9.2[e]	20[e]

[a] All k° values were determined from ΔE_p values corrected for iR_u error and from 5−15 different scan rates per sample. [b] Values in parentheses are the relative standard deviation of the mean for 2−4 different films. [c] From ref 45. [d] This work. [e] From ref 22. [f] From ref 44.

The electrode capacitance values (C°) reported in Table 2 were obtained from cyclic voltammograms in 1 M KCl at a variety of scan rates (0.1−5 V/s). In all cases, background current in cyclic voltammograms and measured C° values at ECFs are lower than GC. This is predominantly due to the significantly smoother surface of the ECFs. The capacitance at the 200-nm films is very similar to that of a smooth Hg surface (~20 μF/cm^2). The lower C° values at the 7-nm films may be attributed to space charge effects as is observed at the basal plane of ordered graphite.[40] Importantly, the low background current reflected in the C° values at the ECFs does not come at the expense of lower ET reactivity.

DISCUSSION

Several techniques have been reported in the literature for preparing thin carbon films. Examples of these include thermal decomposition of gaseous precursors,[11] e-beam evaporation,[17,18,34,36,37] vacuum sputtering,[15,16] and pyrolysis of thin films of polymers.[19,21−23] While films prepared by a number of procedures have been examined as electrodes, the electrochemical performance of films deposited by e-beam evaporation has not been thoroughly studied. The application of e-beam-deposited carbon films for use as optically transparent electrodes was reported a number of years ago.[17,18] These films, deposited on glass or quartz, had two significant shortcomings as electrodes: poor adhesion to the substrate and high electrode resistance. The electrode fabrication technique presented here overcomes these difficulties. Specifically, the use of highly doped silicon without an oxide layer as the substrate overcomes the previous challenges with both film adhesion and poor film conductivity. The strong interaction between the carbon- and oxide-free Si form an interfacial SiC layer[34] that both increases adhesion and promotes good electrical contact between the conductive substrate and the carbon film.

In terms of electrochemical reactivity, ECFs compare favorably with GC. Pyrolyzed ECFs exhibit ET rates similar to or higher than GC for outer-sphere redox systems. The rate constants measured of ECFs for surface-sensitive redox probes indicate a comparable surface chemistry. In addition, the magnitudes of electrode capacitance and 2,6-AQDS surface coverage are similar to what one would expect at a smooth GC surface. The redox species examined here were chosen to probe the various structural and chemical aspects that have been shown to be important at carbon electrodes.[2,40] Except for PPF, no other type of carbon film has been characterized as extensively. The ET kinetics of $Fe(CN)_6^{3-/4-}$ have been measured at a number of different types of carbon thin films enabling the direct comparison presented in Table 3. Table 3 shows that the pyrolyzed 200-nm ECFs yield among the highest rates measured at thin carbon film electrodes.

Table 3. Comparison of $Fe(CN)_6^{3-/4-}$ ET Kinetics at Carbon Film Electrodes

type of film	k° for $Fe(CN)_6^{3-/4-}$ (cm/s)	ref
e-beam deposited on glass (28 nm)	1.2×10^{-3}[a] (1 M KNO_3)[b]	17
pyrolyzed on Macor	$3.8-15.4 \times 10^{-3}$ (1 M KCl)	19
sputtered	$2.4-4.2 \times 10^{-2}$ (0.5 M H_2SO_4)	15
CVD of natural gas on quartz	1.6×10^{-3} (0.1 M KNO_3)	11
CVD of ethane on GC	5×10^{-3} (1 M KCl)	12
pyrolyzed negative photoresist	1.8×10^{-2},[a] (1 M KNO_3)	23
PPF	1.2×10^{-2} (1 M KCl)	22
pyrolyzed 200-nm ECF	2.9×10^{-2} (1 M KCl)	this work

[a] Calculated from reported ΔE_p values. [b] Electrolyte solution used.

Electrode flatness is crucial for the use of carbon films in applications such as molecular electronics. Another line of research that will benefit from ultraflat carbon surfaces is scanning probe microscopic (SPM) studies of adsorbed materials. For example, pyrolytic carbon is commonly used as an artificial heart valve material;[49] however, the roughness of the material prohibits SPM studies of adsorbed proteins that may lend insight into biocompatibility issues. Although highly ordered pyrolytic graphite (HOPG) has been used as a substrate for protein adsorption studies,[50] the microstructure of HOPG is not a good model for pyrolytic carbon.

(49) Feng, L.; Andrade, J. D. *Biomaterials* **1994**, *15*, 323−333.

The SFM studies of the ECF surfaces demonstrated exceptional flatness, with rms roughness values around 1 Å for the nonpyrolyzed films, which is comparable to the flatness of the underlying silicon. Although the composition of extremely flat nonpyrolyzed surfaces is amorphous carbon, they exhibit reasonable electrochemical reactivity. Two previous studies on e-beam carbon films deposited at room temperature have reported higher roughness values of 0.8 [36] and >1 nm[37] though both studies used silicon with a surface oxide layer. As stated previously, carbon films are poorly adhered to glass and other silicon oxide surfaces. Weak interactions between the depositing carbon atoms and the substrate will lead to a three-dimensional island growth mechanism (Volmer−Weber) and an overall rougher surface. We attribute the low roughness of our films to strong interactions between the carbon atoms and clusters formed by the evaporation process and the oxide-free Si⟨100⟩ substrate. The strong interactions lead to the 2D growth of a SiC seed layer. Once the SiC seed layer is established, strong carbon−carbon interactions severely limit the mobility of depositing carbon atoms, induce additional 2D growth, and finally result in films with roughness values growing only marginally with increasing evaporation thickness (as shown in Figure 2A). Pyrolysis of ECFs at 1000 °C induces limited graphite domain formation, increases ET rates, and increases the rms roughness to 0.4−0.6 nm. Although significantly more rough than nonpyrolyzed ECFs, these films are still extremely flat and comparable to PPF.

CONCLUSIONS

We have characterized the microstructure, roughness and electrochemical activity of carbon thin films (≤200 nm) prepared by e-beam evaporation onto oxide-free Si substrates. The films show strong adhesion to the substrate due to the formation of a SiC interfacial layer. Raman spectra indicate that ECFs initially exhibit an amorphous carbon structure and that pyrolysis at 1000 °C results in some graphitic content. The films are compatible with aqueous electrolytes (pH 1 to ∼8 examined here), acetonitrile, and 2-propanol (used to clean the electrodes). Nonpyrolyzed films show reasonable electrochemical activity and exhibit the lowest roughness measured at carbon films (∼0.1 nm). Pyrolysis increases the roughness of the films slightly but produces more electrochemically active surfaces. Electron-transfer rates measure at the pyrolyzed films are comparable to GC and are among the highest reported for carbon thin-film electrodes. These ultrasmooth films should find applications in molecular electronics and SFM studies. An additional advantage of the e-beam evaporation process is the possibility of producing electrode arrays by exploiting conventional lithographic techniques to pattern the surface of the silicon wafer prior to the evaporation of carbon. This opens pathways for a wide range of uniquely patterned ECF films to be explored.

(50) Ta, T. C.; Sykes, M. T.; McDermott, M. T. *Langmuir* **1998**, *14*, 2435−2443.

ACKNOWLEDGMENT

The Natural Sciences and Engineering Research Council of Canada (NSERC) and the Department of Chemistry, University of Alberta supported this work. The Raman spectroscopy carried out at Ohio State was supported by the National Science Foundation through Project 0211693 from the Analytical and Surface Chemistry Division. A.A.R. thanks the University of Mazandaran for sabbatical leave support. J.J.B. gratefully acknowledges NSERC and iCORE for their support.

Received for review August 26, 2003. Accepted February 19, 2004.

AC035003J